Acoustic Realization of Quadrupole Topological Insulators

Yajuan Qi,[1] Chunyin Qiu,[1,*] Meng Xiao,[1,†] Hailong He,[1,2] Manzhu Ke,[1,2] and Zhengyou Liu[1,2]
[1]Key Laboratory of Artificial Micro- and Nano-Structures of Ministry of Education and School of Physics and Technology, Wuhan University, Wuhan 430072, China
[2]Institute for Advanced Studies, Wuhan University, Wuhan 430072, China

(Received 6 December 2019; accepted 29 April 2020; published 18 May 2020)

A quadrupole topological insulator, being one higher-order topological insulator with nontrivial quadrupole quantization, has been intensely investigated very recently. However, the tight-binding model proposed for such emergent topological insulators demands both positive and negative hopping coefficients, which imposes an obstacle in practical realizations. Here, we introduce a feasible approach to design the sign of hopping in acoustics, and construct the first acoustic quadrupole topological insulator that stringently emulates the tight-binding model. The inherent hierarchy quadrupole topology has been experimentally confirmed by detecting the acoustic responses at the bulk, edge, and corner of the sample. Potential applications can be anticipated for the topologically robust in-gap states, such as acoustic sensing and energy trapping.

DOI: 10.1103/PhysRevLett.124.206601

Introduction.—The past decade has witnessed an explosive development of topological states of matter in classical wave systems [1–5]. The robustness of the topological systems against disorders and the associated one-way edge states provide new opportunities for manipulating classical waves. Besides the analogs of conventional topological insulators [6–24] and topological semimetals [25–34], the recent interest on higher-order topological insulators (HOTIs) [35,36] has opened a new direction of topological phases in classical systems [37–53]. Different from the conventional topological insulators, in which the D-dimensional bulk is gapped and the topological invariant counts the number of gapless modes hosted on the $(D-1)$-dimensional boundaries of the sample, the HOTIs are a new family of topological phases of matter that goes beyond the conventional bulk-boundary correspondence principle. For example, unlike conventional two-dimensional (2D) topological insulators, a 2D second-order HOTI does not exhibit gapless one-dimensional (1D) topological edge states, but instead has topologically protected zero-dimensional (0D) corner states. Because of the flexibility in sample design, HOTIs have been soon implemented in mechanical [37,45], photonic [38,40–44], electrical circuits [39,46,47] and acoustic [48–53] systems.

A quadrupole topological insulator (QTI) [35,36], featuring a nontrivial quadrupole moment, has drawn extensive attention recently [37–39,41]. In this novel 2D topological system, a bulk quadrupole moment in a finite-sized sample gives rise to surface dipole moments on its 1D edges and to uncompensated charges on the 0D corners. The former contributes to gapped edge modes and the latter exhibits the presence of nontrivial corner modes, which reflects an exotic hierarchy topological inherent in the QTIs [35,36]. Comparing with the other 2D HOTIs, the corner states of QTIs are stably pinned to the middle of the bulk gap due to the inherent chiral symmetries, and thus persist as long as the bulk band exhibits nontrivial quadrupole moment. Though broad attention received, experimental studies on such 2D QTIs are still rather limited [37–39,41]. The QTI theory proposed with a square-lattice tight-binding (TB) model [35,36] requires a π flux per plaquette. This demands both positive and negative hoppings in a spinless and time-reversal invariant classical system, where the hoppings must be real valued. However, fulfilling this harsh requirement usually involves fine-tuning of the parameters [37,41,54], and hence hinders the experimental implementation of the classical QTIs. In particular, so far there is no experimental progress reported for acoustic QTIs, since there is no feasible route proposed to control the sign of acoustic couplings.

In this Letter, we conceive a simple mechanism to generate both positive and negative hoppings in acoustics. That is, linking acoustic cavities with different connectivity according to the field morphologies of acoustic resonators. After testing the design route of controlling hoppings, we present an experimental realization of the acoustic QTI that stringently fulfills the 2D TB model proposed for QTIs [35,36]. The hierarchy topology of our acoustic QTI has been conclusively identified through detecting the acoustic responses at the bulk, edge, and corner. In particular, our acoustic QTI exhibits a big bulk gap and the topological corner states are well separated from the gapped edge and bulk states, which is crucial in practical applications such as creating topologically stable acoustic enhancement. All experimental data agree excellently with our numerical simulations performed with COMSOL Multiphysics.

Design route of positive and negative hoppings in acoustics.—As stated above, a prerequisite for realizing acoustic QTIs is to design positive and negative hoppings independently. So far, there is no explicit route conceived to accomplish this goal, despite the fact that TB models have been frequently implemented in acoustics. Here, we start from two identical resonators connected with a coupler, associated with effective Hamiltonian

$$H = \begin{pmatrix} \omega_0 & \kappa \\ \kappa & \omega_0 \end{pmatrix}, \tag{1}$$

in which ω_0 is the frequency of the two resonators, and κ represents a real-valued coupling coefficient between them. The composed system exhibits split eigenfrequencies $\omega_\pm = \omega_0 \pm \kappa$ associated with eigenvectors $(1/\sqrt{2})(1, \pm 1)^T$: the signs $+$ and $-$ characterize the modes formed by in-phase and out-of-phase couplings, respectively. Therefore, a negative (positive) coupling κ suggests that the in-phase coupled mode has an energy lower (higher) than that of out-of-phase one. This is illustrated in Figs. 1(a) and 1(b) by a coupled P_z-dipole system. In acoustics, both configurations can be implemented by a pair of identical air cavities coupled with narrow tubes, which are distinguished with straight-linked and cross-linked connectivity, as shown in Figs. 1(c) and 1(d). Physically, the cavity resonators emulate atomic orbitals and the narrow tubes introduce hoppings between them. Here, the cavity parameters $l = 8.12$ cm, $w = 6.90$ cm, and $h = 10.45$ cm are selected to ensure the frequency of the P_z mode (1627 Hz) far away from the other cavity modes (Supplemental Material [55]).

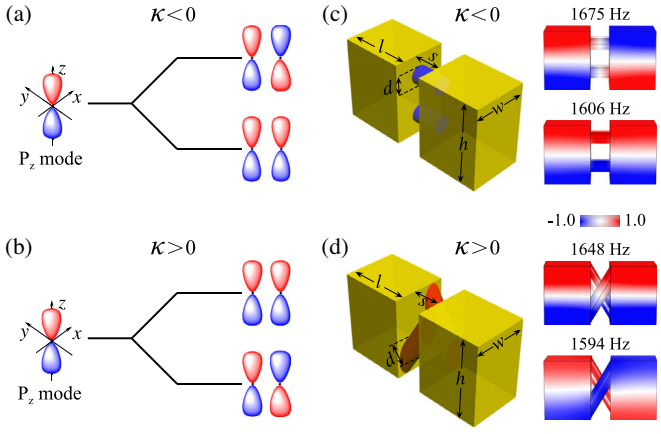

FIG. 1. (a),(b) Sketches of the split energy levels for two coupled P_z dipoles with hoppings $\kappa < 0$ and $\kappa > 0$, respectively. For the case of $\kappa < 0$ ($\kappa > 0$), the in-phase coupled mode has an energy lower (higher) than that of out-of-phase one. (c),(d) Acoustic realizations of the negative and positive hoppings with coupled resonators, respectively. Left: Double cavity structures coupled with different connectivity. The resonance cavities (yellow) and narrow tubes (red or blue) are filled with air and bounded with hard boundaries. Right: Pressure distributions at given eigenfrequencies.

When the air cavities are straightly connected with two identical tubes (of diameter $d = 2.32$ cm and length $s = 3.48$ cm, at a distance of $h/4$ to the top or bottom surface), the composed system exhibits an in-phase coupled P_z mode at a frequency (1606 Hz) lower than that of the out-of-phase one (1675 Hz). That is, the straight-linked system has a negative coupling for P_z modes. By contrast, the system exhibits a positive coupling when the cavities are crosswise connected, in which the in-phase coupled mode occurs at a frequency (1648 Hz) higher than that of the out-of-phase one (1594 Hz). Note that the hopping strengths depend mostly on the sizes and positions of the narrow tubes, and the central frequencies of the coupled systems may shift from the single cavity resonance due to the introduction of coupling tubes (Supplemental Material [55]).

Experimental identification of the sign of the designed hoppings.—The design route for achieving desired hopping sign was confirmed in our airborne sound experiments. Figures 2(a) and 2(b) show the experimental setups. The samples were fabricated precisely via a mature 3D-printing technique with photosensitive resin, which can be safely viewed as acoustically rigid for airborne sound. For each case, a broadband pointlike sound source, launched from a subwavelength-sized tube, was injected into the right cavity from the backside, and the pressure responses of four typical positions were detected through the holes (of radii ~0.4 cm) perforated in the front of the sample, which were sealed when not in use. Figures 2(c) and 2(d) present the measured amplitude spectra (color circles) for the straight-linked and cross-linked systems, respectively, together with the simulation results (color lines) for comparison. (Each amplitude spectrum was normalized by the measurement without sample and then rescaled to its maximum.) As expected, in each case two resonance peaks emerge near the eigenfrequencies (green arrows) of the coupled P_z modes. Figures 2(e) and 2(f) present the phase spectra under the reference of the position 4, which show clearly a phase difference $\sim\pi$ between the positions 1 and 2 (or 3 and 4), an indication of the P_z modes in both configurations. In particular, for the straight-linked cavity structure [Fig. 1(e)], the phase difference between the positions 1 and 3 (or 2 and 4) approaches zero at the lower frequency while approaches π at the higher frequency. This concludes unambiguously a negative hopping since the in-phase coupled mode occurs at the lower frequency than that of out-of-phase one. In contrast, for the cross-linked structure [Fig. 1(f)], the phase responses indicate an in-phase mode at the higher frequency and thus conclude a positive hopping. All the experiments match quantitatively with the simulations. It is worth pointing out that here we take advantage of the unique field profile of the P_z mode to achieve positive and negative hoppings independently. In fact, the cavity also supports the P_x dipole at a higher frequency; however, both configurations contribute positive hoppings for the P_x mode (Supplemental Material [55]).

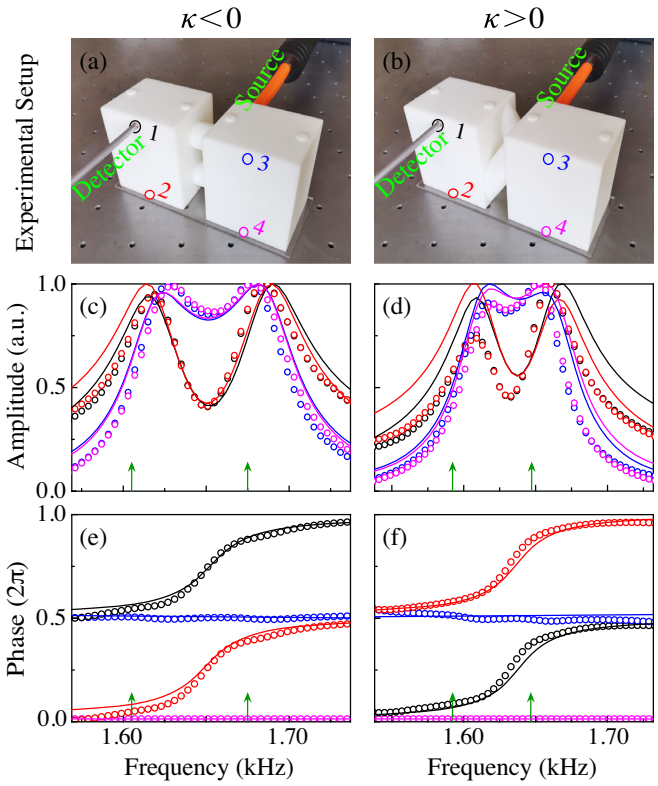

FIG. 2. (a),(b) Experimental setups for testing the hopping signs of the straight-linked and cross-linked double cavity systems, respectively. The acoustic signal is injected from the backside of the sample, and four typical positions (labeled with color circles) in the front are used for detection. (c),(d) Measured (circles) and simulated (lines) pressure amplitude responses at the four locations (plotted with consistent color). The green arrows indicate the eigenfrequencies of the coupled P_z modes. (e),(f) The associated phase spectra.

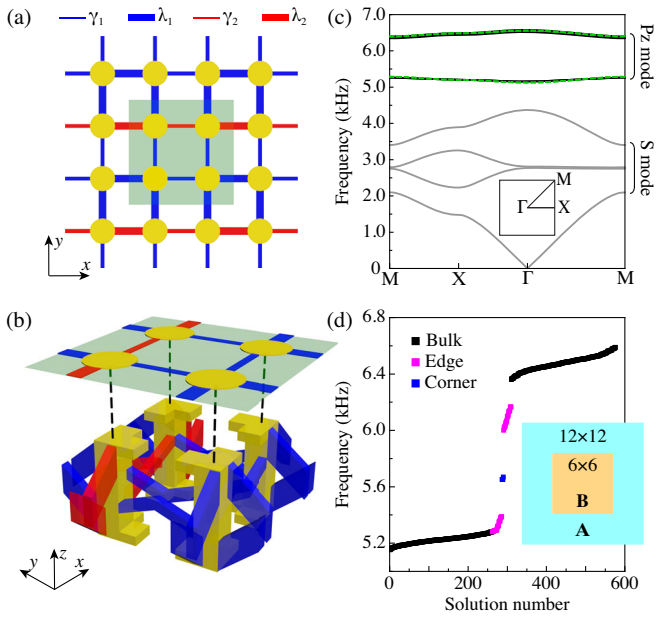

FIG. 3. (a) Square-lattice TB model with positive (red) and negative (blue) nearest-neighbor hoppings $\lambda_{1,2}$ and $\gamma_{1,2}$, where the shaded square sketches a four-site unit cell. This hoping distribution results in a π flux per plaquette. (b) Unit structure of our acoustic system that emulates the TB model: yellow for resonant cavities, and blue and red for coupling tubes. (c) Band structure. The P_z bands (black solid lines) are captured well by the TB model (green dashed lines). Inset: the first Brillouin zone of the square lattice. (d) Eigenvalue spectrum for a finite-sized sample constructed with the topologically distinct quadruple phases **A** and **B** (inset), identified with bulk, edge, and corner states through inspecting eigenfields.

Acoustic QTI and topological in-gap states.—Our design starts from the square-lattice TB model for QTI theory [35,36]. As sketched in Fig. 3(a), each unit cell contains four sublattices: the yellow disks represent lattice sites and the bonds are hoppings between them. For a spinless and time-reversal invariant system, the hoppings can only be real, either positive or negative. Considering the fact that each plaquette possesses a flux of π, the hoppings herein cannot be all positive or negative. Figure 3(a) shows one configuration that satisfies this requirement, providing that the intracell hoppings $\gamma_2 = -\gamma_1$ and the intercell hoppings $\lambda_2 = -\lambda_1$. In particular, the unit cell exhibits a nonzero quadrupole moment if $|\lambda_{1,2}| > |\gamma_{1,2}|$ and zero quadrupole moment if $|\lambda_{1,2}| < |\gamma_{1,2}|$. These two topologically distinct quadrupole phases, denoted by **A** and **B** for brevity, can be constructed directly in acoustic systems following the above design route for positive and negative hoppings. As exhibited above, the signs of the acoustic hoppings can be controlled by the connectivity of the coupling tubes, the strengths of hoppings can be engineered by tuning the positions and sizes of the coupling tubes, and the onsite energy depends mostly by the geometry of cavity resonators. As such, topologically distinct quadrupole insulators can be achieved by tailoring the geometric parameters of the coupling tubes. In fact, the phase **B** can be simply realized by switching the values of the inter- and intracell hoppings predesigned for the phase **A**, associated with the same band structure. According to the generalized bulk-boundary correspondence [35,36], topologically protected in-gap states can be observed at the edges and corners formed between **A** and **B**, as to be shown in Fig. 3(d).

Figure 3(b) shows the unit structure of our acoustic QTI. It has an in-plane lattice constant of 4.2 cm and a finite height of 2.0 cm in the z direction. Critically, the designed acoustic structure carries positive (red) and negative (blue) hoppings, which are distributed according to the TB model in Fig. 3(a). The elementary structures are a bit more complex than those presented in Fig. 1, in order to satisfy the TB model in a quantitative way (see details in Supplemental Material [55]). Figure 3(c) shows the band structure for this acoustic system. The lower four bands (gray solid lines) are formed by the S modes featured with uniform field patterns inside the cavities. In contrast, the upper four bands (black solid lines) are formed exactly by

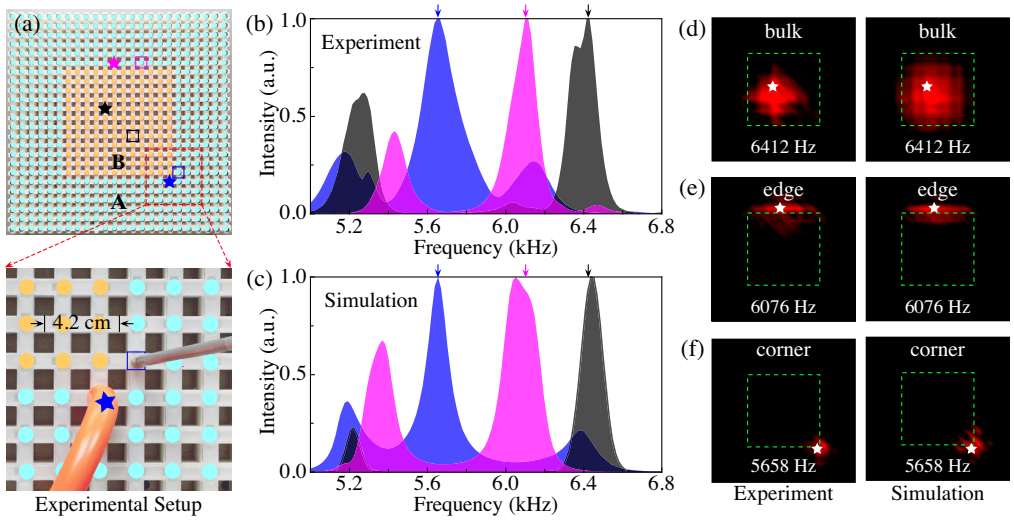

FIG. 4. (a) Experimental setup for identifying the hierarchy quadrupole topology. Upper panel: experimental sample. Lower panel: an enlarged picture for demonstrating the pump-probe measurement of the corner response. The color stars and squares label, respectively, the positions of the source and detector when measuring the bulk (black), edge (purple), and corner (blue) responses. (b) Experimentally measured bulk (black), edge (purple), and corner (blue) spectra. (c) Numerical comparison of (b). (d)–(f) Measured and simulated pressure amplitude distributions for the bulk, edge, and corner states, respectively, plotted in logarithmic scale with bright (dark) for strong (weak) field. The frequencies correspond to the peaks labeled in (b) and (c). In each case, the white star indicates the position of the acoustic source.

P_z modes, each two of which are nearly doubly degenerate. All the P_z bands are captured precisely by the TB model (green dashed lines) with fitting parameters $\lambda_1 = -\lambda_2 = -455$ Hz, $\gamma_1 = -\gamma_2 = -57$ Hz, and the onsite energy 5830 Hz. Remarkably, a big omnidirectional band gap (~1060 Hz, associated with a gap-to-midgap ratio ~18%) emerges between the two pairs of P_z bands, which is induced by the strong dimerization ($|\lambda_{1,2}|/|\gamma_{1,2}| \approx 8.0$) and matches well the value $2\sqrt{2}(|\lambda_{1,2}| - |\gamma_{1,2}|)$ derived from the TB model (Supplemental Material [55]). In order to demonstrate the higher-order topological effect, in Fig. 3(d) we present the simulated eigenfrequency spectrum for a finite-sized sample (12×12 unit cells in total, see inset). As expected, it shows clearly the coexistence of the topologically protected 1D edge states and 0D corner states inside the bulk gap. Physically, both the topological in-gap states are originated in the bulk topology of the QTI: the gapped edge states stem from the nontrivial surface dipole quantization, whereas the topological corner states come from the nontrivial quadrupole quantization [35,36]. (As such, these in-gap topological responses depend mostly on the geometries of the coupling tubes.) In particular, the big bulk gap and the spectrally well-isolated topological corner states greatly facilitate the experimental characterization of the cascade hierarchy of quadrupole topology in our system. Note that the corner modes are not perfectly degenerate (associated with a frequency split ~1.7% with respect to the bulk gap), because of the unavoidable next-nearest-neighbor coupling or coupling to other bands [37,56], which is beyond the description of the TB model presented in Refs. [35,36].

Experimental demonstration of the hierarchy quadrupole topology.—The higher-order topology of the acoustic QTI was identified by our experiments. Figure 4(a) shows the experimental setup. As considered in Fig. 3(d), our sample has a size of 12×12 unit cells (576 resonators in total), where the site cavities were colored to distinguish the topologically different quadrupole phases **A** and **B**. To map out the 2D field profiles, each site cavity was perforated with a hole (sealed when not in use) for inserting the acoustic source or detector. To confirm the coexistence of the bulk, edge, and corner modes, we first measured the frequency-resolved acoustic responses for three typical pump-probe configurations. In each case, the positions of the acoustic source and detector are highlighted by the color star and square [Fig. 4(a)]. Figure 4(b) shows the corresponding intensity spectra detected for the three independent experiments. As expected, the bulk spectrum (black) exhibits two intensity peaks (centered at 5260 and 6412 Hz) and identifies the wide bulk gap between the two pairs of P_z bands in Fig. 3(c). The edge spectrum (purple) exhibits two peaks (around 5410 and 6076 Hz) within the bulk gap, which correspond exactly to the gapped 1D edge states. By contrast, in addition to the minor peaks contributed from the bulk and edge states, the corner spectrum (blue) shows one prominent peak (centered at 5658 Hz) inside the common gap of the edge and bulk states, which serves as unambiguous evidence for the presence of topological corner states. (The peak broadening mainly comes from the unavoidable material absorption and fabrication error of the sample.) All the spectra match excellently the simulation results presented in Fig. 4(c), in

which a uniform dispassion loss was used (Supplemental Material [55]). To conclusively verify the cascade hierarchy of high-order topology, we further scanned and characterized the field distributions at the peak frequencies of the bulk, edge, and corner spectra. As shown in Figs. 4(d)–4(f), the measured field patterns (left panels) directly visualize the features of the bulk, edge, and corner states, respectively, again in good agreement with the numerical results (right panels).

Conclusions.—We have designed an acoustic QTI that follows the TB model proposed for QTI theory, and experimentally validated the hierarchy quadrupole topology through measuring the topological 1D edge states and 0D corner states. The positive and negative hoppings are conceived independently by introducing different connectivity between acoustic resonators. Instead of multipole resonators [37], here dipole resonators are used to achieve a wide bulk gap, which facilitates the experimental characterization of the hierarchy topology of our acoustic QTI. In addition, an arbitrary controlling of the real-valued hoppings enables the further investigation of rich physics inherent in engineering Z_2-gauge flux [54,57,58]. Note that the corner states are topologically stable even in the presence of disorders (see Supplemental Material [55]), as long as the chiral symmetry of the acoustic structure is ensured by its fabrication. This enables a robust and precise control of sound energy concentration, and thus points to a wide range of application avenues that demand highly localized strong sound fields, such as sound energy harvesting, acoustic sensing, and trapping microparticles by acoustic radiation force.

C. Q. is supported by the Young Top-notch Talent for Ten Thousand Talent Program and National Natural Science Foundation of China (Grant No. 11774275); M. X. is supported by the National Natural Science Foundation of China (Grant No. 11904264) and the startup funding of Wuhan University; Z. L. is supported by the National Key R&D Program of China (Grant No. 2018YFA0305800) and the National Natural Science Foundation of China (Grants No. 11890701 and No. 11674250).

Note added.—Recently, we became aware of one work that realized acoustic QTIs based on the nonsymmorphic symmetry of sonic crystals [59]; we also notice that similar approaches were introduced to construct acoustic octupole topological insulators [60,61].

*Corresponding author.
cyqiu@whu.edu.cn,
†Corresponding author.
phmxiao@whu.edu.cn

[1] T. Ozawa, H. M. Price, A. Amo, N. Goldman, M. Hafezi, L. Lu, M. Rechtsman, D. Schuster, J. Simon, O. Zilberberg, and I. Carusotto, Topological photonics, Rev. Mod. Phys. **91**, 015006 (2019).
[2] G. Ma, M. Xiao, and C. T. Chan, Topological phases in acoustic and mechanical systems, Nat. Rev. Phys. **1**, 281 (2019).
[3] X. Zhang, M. Xiao, Y. Cheng, M.-H. Lu, and J. Christensen, Topological sound, Commun. Phys. **1**, 97 (2018).
[4] L. Lu, J. D. Joannopoulos, and M. Soljacic, Topological photonics, Nat. Photonics **8**, 821 (2014).
[5] S. D. Huber, Topological mechanics, Nat. Phys. **12**, 621 (2016).
[6] F. D. M. Haldane and S. Raghu, Possible Realization of Directional Optical Waveguides in Photonic Crystals with Broken Time-Reversal Symmetry, Phys. Rev. Lett. **100**, 013904 (2008).
[7] Z. Wang, Y. Chong, J. Joannopoulos, and M. Soljacic, Observation of unidirectional backscattering-immune topological electromagnetic states, Nature (London) **461**, 772 (2009).
[8] Y. Poo, R. X. Wu, Z. F. Lin, Y. Yang, and C. T. Chan, Experimental Realization of Self-Guiding Unidirectional Electromagnetic edge States, Phys. Rev. Lett. **106**, 093903 (2011).
[9] M. Hafezi, E. A. Demler, M. D. Lukin, and J. M. Taylor, Robust optical delay lines with topological protection, Nat. Phys. **7**, 907 (2011).
[10] K. Fang, Z. Yu, and S. Fan, Realizing effective magnetic field for photons by controlling the phase of dynamic modulation, Nat. Photonics **6**, 782 (2012).
[11] A. B. Khanikaev, S. H. Mousavi, W.-K. Tse, M. Kargarian, A. H. MacDonald, and G. Shvets, Photonic topological insulators, Nat. Mater. **12**, 233 (2013).
[12] M. C. Rechtsman, J. M. Zeuner, Y. Plotnik, Y. Lumer, D. Podolsky, F. Dreisow, S. Nolte, M. Segev, and A. Szameit, Photonic Floquet topological insulators, Nature (London) **496**, 196 (2013).
[13] W. Chen, S.-J. Jiang, X.-D. Chen, B. Zhu, L. Zhou, J.-W. Dong, and C. T. Chan, Experimental realization of photonic topological insulator in a uniaxial metacrystal waveguide, Nat. Commun. **5**, 5782 (2014).
[14] L. Wu and X. Hu, Scheme for Achieving a Topological Photonic Crystal by Using Dielectric Material, Phys. Rev. Lett. **114**, 223901 (2015).
[15] X. Cheng, C. Jouvaud, X. Ni, S. H. Mousavi, A. Z. Genack, and A. B. Khanikaev, Robust reconfigurable electromagnetic pathways within a photonic topological insulator, Nat. Mater. **15**, 542 (2016).
[16] L. J. Maczewsky, J. M. Zeuner, S. Nolte, and A. Szameit, Observation of photonic anomalous Floquet topological insulators, Nat. Commun. **8**, 13756 (2017).
[17] R. Süsstrunk and S. D. Huber, Observation of phononic helical edge states in a mechanical topological insulator, Science **349**, 47 (2015).
[18] Z. Yang, F. Gao, X. Shi, X. Lin, Z. Gao, Y. Chong, and B. Zhang, Topological Acoustics, Phys. Rev. Lett. **114**, 114301 (2015).
[19] C. He, X. Ni, H. Ge, X.-C. Sun, Y.-B. Chen, M.-H. Lu, X.-P. Liu, and Y.-F. Chen, Acoustic topological insulator and robust one-way transport, Nat. Phys. **12**, 1124 (2016).

[20] R. Fleury, A. B. Khanikaev, and A. Alu, Floquet topological insulators for sound, Nat. Commun. **7**, 11744 (2016).
[21] Y. G. Peng, C. Z. Qin, D. G. Zhao, Y. X. Shen, X. Y. Xu, M. Bao, H. Jia, and X. F. Zhu, Experimental demonstration of anomalous Floquet topological insulator for sound, Nat. Commun. **7**, 13368 (2016).
[22] J. Lu, C. Qiu, L. Ye, X. Fan, M. Ke, F. Zhang, and Z. Liu, Observation of topological valley transport of sound in sonic crystals, Nat. Phys. **13**, 369 (2017).
[23] J. Lu, C. Qiu, W. Deng, X. Huang, F. Li, F. Zhang, S. Chen, and Z. Liu, Valley Topological Phases in Bilayer Sonic Crystals, Phys. Rev. Lett. **120**, 116802 (2018).
[24] Y. Ding, Y. Peng, Y. Zhu, X. Fan, J. Yang, B. Liang, X. Zhu, X. Wan, and J. Cheng, Experimental Demonstration of Acoustic Chern Insulators, Phys. Rev. Lett. **122**, 014302 (2019).
[25] L. Lu, Z. Wang, D. Ye, L. Ran, L. Fu, J. D. Joannopoulos, and M. Soljačić, Experimental observation of Weyl points, Science **349**, 622 (2015).
[26] M. Xiao, W. Chen, W. He, and C. T. Chan, Synthetic gauge flux and Weyl points in acoustic systems, Nat. Phys. **11**, 920 (2015).
[27] W.-J. Chen, M. Xiao, and C. T. Chan, Phononic crystals possessing multiple Weyl points and the experimental observation of robust surface states, Nat. Commun. **7**, 13038 (2016).
[28] H. He, C. Qiu, L. Ye, X. Cai, X. Fan, M. Ke, F. Zhang, and Z. Liu, Topological negative refraction of surface acoustic waves in a Weyl phononic crystal, Nature (London) **560**, 61 (2018).
[29] F. Li, X. Huang, J. Lu, J. Ma, and Z. Liu, Weyl points and Fermi arcs in a chiral phononic crystal, Nat. Phys. **14**, 30 (2018).
[30] H. Ge, X. Ni, Y. Tian, S. K. Gupta, M.-H. Lu, X. Lin, W.-D. Huang, C. T. Chan, and Y.-F. Chen, Experimental Observation of Acoustic Weyl Points and Topological Surface States, Phys. Rev. Applied **10**, 014017 (2018).
[31] B. Yang *et al.*, Ideal Weyl points and helicoid surface states in artificial photonic crystal structures, Science **359**, 1013 (2018).
[32] W. Gao, B. Yang, B. Tremain, H. Liu, Q. Guo, L. Xia, A. P. Hibbins, and S. Zhang, Experimental observation of photonic nodal line degeneracies in metacrystals, Nat. Commun. **9**, 950 (2018).
[33] Q. Guo, O. You, B. Yang, J. B. Sellman, E. Blythe, H. Liu, Y. Xiang, J. Li, D. Fan, J. Chen, C. T. Chan, and S. Zhang, Observation of Three-Dimensional Photonic Dirac Points and Spin-Polarized Surface Arcs, Phys. Rev. Lett. **122**, 203903 (2019).
[34] X. Fan, C. Qiu, Y. Shen, H. He, M. Xiao, M. Ke, and Z. Liu, Probing Weyl Physics with One-Dimensional Sonic Crystals, Phys. Rev. Lett. **122**, 136802 (2019).
[35] W. A. Benalcazar, B. A. Bernevig, and T. L. Hughes, Electric multipole moments, topological multipole moment pumping, and chiral hinge states in crystalline insulators, Phys. Rev. B **96**, 245115 (2017).
[36] W. A. Benalcazar, B. A. Bernevig, and T. L. Hughes, Quantized electric multipole insulators, Science **357**, 61 (2017).
[37] M. Serra-Garcia, V. Peri, R. Süsstrunk, O. R. Bilal, T. Larsen, L. G. Villanueva, and S. D. Huber, Observation of a phononic quadrupole topological insulator, Nature (London) **555**, 342 (2018).
[38] C. W. Peterson, W. A. Benalcazar, T. L. Hughes, and G. Bahl, A quantized microwave quadrupole insulator with topologically protected corner states, Nature (London) **555**, 346 (2018).
[39] S. Imhof, C. Berger, F. Bayer, J. Brehm, L. W. Molenkamp, T. Kiessling, F. Schindler, C. H. Lee, M. Greiter, T. Neupert, and R. Thomale, Topolectrical-circuit realization of topological corner modes, Nat. Phys. **14**, 925 (2018).
[40] J. Noh, W. A. Benalcazar, S. Huang, M. J. Collins, K. P. Chen, T. L. Hughes, and M. C. Rechtsman, Topological protection of photonic mid-gap defect modes, Nat. Photonics **12**, 408 (2018).
[41] S. Mittal, V. V. Orre, G. Zhu, M. A. Gorlach, A. Poddubny, and M. Hafezi, Photonic quadrupole topological phases, Nat. Photonics **13**, 692 (2019).
[42] X.-D. Chen, W.-M. Deng, F.-L. Shi, F.-L. Zhao, M. Chen, and J.-W. Dong, Direct Observation of Corner States in Second-Order Topological Photonic Crystal Slabs, Phys. Rev. Lett. **122**, 233902 (2019).
[43] B.-Y. Xie, G.-X. Su, H.-F. Wang, H. Su, X.-P. Shen, P. Zhan, M.-H. Lu, Z.-L. Wang, and Y.-F. Chen, following Letter, Visualization of Higher-Order Topological Insulating Phases in Two-Dimensional Dielectric Photonic Crystals, Phys. Rev. Lett. **122**, 233903 (2019).
[44] A. E. Hassan, F. K. Kunst, A. Moritz, G. Andler, E. J. Bergholtz, and M. Bourennane, Corner states of light in photonic waveguides, Nat. Photonics **13**, 697 (2019).
[45] H. Fan, B. Xia, L. Tong, S. Zheng, and D. Yu, Elastic Higher-Order Topological Insulator with Topologically Protected Corner States, Phys. Rev. Lett. **122**, 204301 (2019).
[46] S. Liu, W. Gao, Q. Zhang, S. Ma, L. Zhang, C. Liu, Y. J. Xiang, T. J. Cui, and S. Zhang, Topologically protected edge state in two-dimensional Su–Schrieffer–Heeger circuit, Research **2019**, 8609875 (2019).
[47] M. Serra-Garcia, R. Süsstrunk, and S. D. Huber, Observation of quadrupole transitions and edge mode topology in an LC circuit network, Phys. Rev. B **99**, 020304(R) (2019).
[48] H. Xue, Y. Yang, F. Gao, Y. Chong, and B. Zhang, Acoustic higher-order topological insulator on a kagome lattice, Nat. Mater. **18**, 108 (2019).
[49] X. Ni, M. Weiner, A. Alù, and A. B. Khanikaev, Observation of higher-order topological acoustic states protected by generalized chiral symmetry, Nat. Mater. **18**, 113 (2019).
[50] X. Zhang, H.-X. Wang, Z.-K. Lin, Y. Tian, B. Xie, M.-H. Lu, Y.-F. Chen, and J.-H. Jiang, Second-order topology and multidimensional topological transitions in sonic crystals, Nat. Phys. **15**, 582 (2019).
[51] Z. Zhang, H. Long, C. Liu, C. Shao, Y. Cheng, X. Liu, and J. Christensen, Deep-subwavelength Holey acoustic second-order topological insulators, Adv. Mater. **31**, 1904682 (2019).
[52] X. Zhang, B. Xie, H. Wang, X. Xu, Y. Tian, J.-H. Jiang, M.-H. Lu, and Y.-F. Chen, Dimensional hierarchy of higher-order topology in three-dimensional sonic crystals, Nat. Commun. **10**, 5331 (2019).
[53] M. Weiner, X. Ni, M. Li, A. Alù, and A. B. Khanikaev, Demonstration of a 3rd order hierarchy of higher order

topological states in a three-dimensional acoustic metamaterial, Sci. Adv. **6**, eaay4166 (2020).

[54] R. Keil, C. Poli, M. Heinrich, J. Arkinstall, G. Weihs, H. Schomerus, and A. Szameit, Universal Sign Control of Coupling in Tight-Binding Lattices, Phys. Rev. Lett. **116**, 213901 (2016).

[55] See Supplemental Material at http://link.aps.org/supplemental/10.1103/PhysRevLett.124.206601 for more details.

[56] K. H. Matlack, M. Serra-Garcia, A. Palermo, S. D. Huber, and C. Daraio, Designing perturbative metamaterials from discrete models, Nat. Mater. **17**, 323 (2018).

[57] S. Rachel, L. Fritz, and M. Vojta, Landau Levels of Majorana Fermions in a Spin Liquid, Phys. Rev. Lett. **116**, 167201 (2016).

[58] M. Kremer, I. Petrides, E. Meyer, M. Heinrich, O. Zilberberg, and A. Szameit, Non-quantized square-root topological insulators: A realization in photonic Aharonov-Bohm cages, Nat. Commun. **11**, 907 (2020).

[59] X. Zhang, Z. Lin, H. Wang, Z. Xiong, Y. Tian, M.-H. Lu, Y.-F. Chen, and J.-H. Jiang, Symmetry-protected hierarchy of anomalous multipole topological band gaps in nonsymmorphic metacrystals, Nat. Commun. **11**, 65 (2020).

[60] X. Ni, M. Li, M. Weiner, A. Alù, and A. B. Khanikaev, Demonstration of a quantized acoustic octupole topological insulator, arXiv:1911.06469.

[61] H. Xue, Y. Ge, H.-X. Sun, Q. Wang, D. Jia, Y.-J. Guan, S.-Q. Yuan, Y. Chong, and B. Zhang, Quantized octupole acoustic topological insulator, arXiv:1911.06068.